Journal of Zhejiang University-SCIENCE C (Computers & Electronics)
ISSN 1869-1951 (Print); ISSN 1869-196X (Online)
www.zju.edu.cn/jzus; www.springerlink.com
E-mail: jzus@zju.edu.cn

Brain tissue segmentation based on spatial information fusion by Dempster-Shafer theory[#]

Jamal GHASEMI[†1], Mohammad Reza KARAMI MOLLAEI[1], Reza GHADERI[1], Ali HOJJATOLESLAMI[2]

([1]*Signal Processing Laboratory, Faculty of Electrical and Computer Engineering, Babol University of Technology, P.O. Box 484, Babol, Iran*)

([2]*School of Computing, University of Kent, Canterbury CT2 7PD, UK*)

[†]E-mail: jghasemi@stu.nit.ac.ir

Received Oct. 7, 2011; Revision accepted Apr. 13, 2012; Crosschecked May 4, 2012

Abstract: As a result of noise and intensity non-uniformity, automatic segmentation of brain tissue in magnetic resonance imaging (MRI) is a challenging task. In this study a novel brain MRI segmentation approach is presented which employs Dempster-Shafer theory (DST) to perform information fusion. In the proposed method, fuzzy c-mean (FCM) is applied to separate features and then the outputs of FCM are interpreted as basic belief structures. The salient aspect of this paper is the interpretation of each FCM output as a belief structure with particular focal elements. The results of the proposed method are evaluated using Dice similarity and Accuracy indices. Qualitative and quantitative comparisons show that our method performs better and is more robust than the existing method.

Key words: Magnetic resonance imaging (MRI), Segmentation, Fuzzy c-mean (FCM), Dempster-Shafer theory (DST)
doi:10.1631/jzus.C1100288 **Document code:** A **CLC number:** TP391

1 Introduction

Magnetic resonance imaging (MRI) is a non-invasive technique to obtain high resolution images which have high intensity contrast between different soft tissues. This imaging technique plays a pivotal role in brain tissue visualization. Brain MRI segmentation (BMS) is an important processing technique in which a region of the MR image with a specific characteristic is labeled. This BMS processing step is of crucial importance in many areas of medical research and in clinical applications where decision making is critical. Automatic segmentation of brain tissue is important in the study of various brain abnormalities, brain development, and evaluation of the progress of treatment.

The main tissues in a normal brain are: gray matter (GM), white matter (WM), and cerebro-spinal fluid (CSF). A brain MRI is a set of images that contain large volumes of information, and therefore manual BMS is a time consuming task. To deal with the volume of information, an automatic segmentation system with acceptable speed, high accuracy, and generalization capability is needed.

Three main artifacts in MRI are: noise, partial volume effect (PVE), and intensity non-uniformity (INU). The main sources of noise are categorized according to biological and scanner noises introduced in earlier studies (Brechbühler *et al*., 1996; Styner *et al*., 2000; Prima *et al*., 2001). Tissue non-uniformity and limitations in hardware design are the main causes of biological and scanner noises, respectively. PVE is defined as a spectrum of intensities that arise when more than one tissue is present in a given pixel. Increasing image resolution results in lower PVE; however, in most cases this also causes noise levels to increase. INU, also known as the bias field, is a low frequency smoothed artifact which is generated by inhomogeneity of the magnetic field during the scanning process (Simmons *et al*., 1994; Sled *et al*., 1998).

[#] A preliminary version was presented at the 7th Iranian Conference on Machine Vision and Image Processing, Nov. 16–17, 2011, Tehran, Iran

MRI problems that occur during the scanning process typically lead to uncertainty in pixel value interpretation. As shown in Fig. 1, this uncertainty can be up to 30% of the pixel intensity, which leads to a considerable overlap between the intensity values used to identify different tissues (Gispert *et al*., 2004).

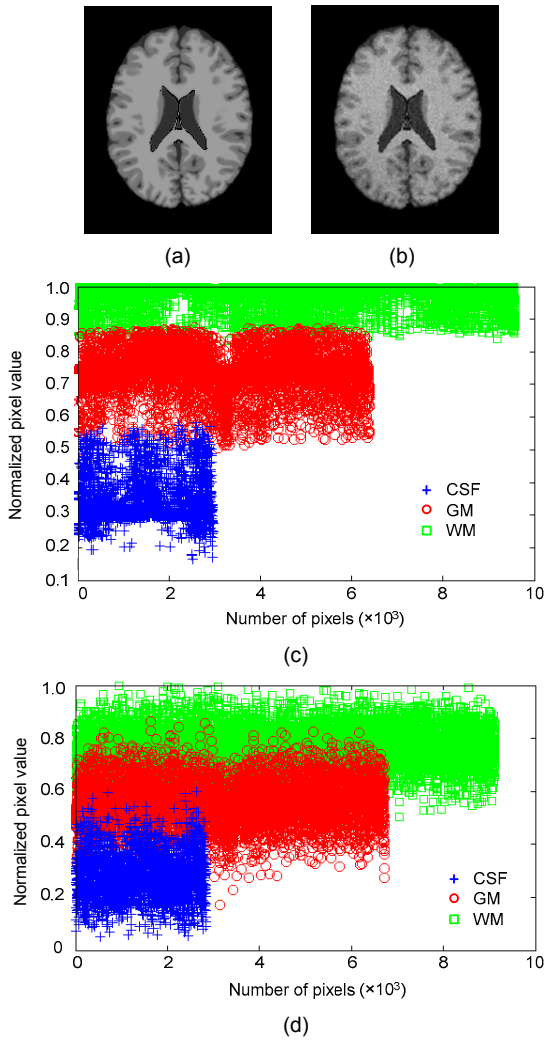

Fig. 1 Tissues overlap in brain magnetic resonance imaging (MRI)

(a) Artifact free (ideal) MRI; (b) Brain MRI with 9% noise and 40% intensity non-uniformity (INU); (c) Intensity distribution of (a); (d) Intensity distribution of (b)

Many researchers have proposed methods to overcome the challenges of BMS (Pham *et al*., 2000; Liew and Yan, 2006). Such methods can be classified into three main categories: boundary-based, region-based, and hybrid (Niessen *et al*., 1999; Wang *et al*., 2008). In boundary-based methods, the gradient features close to an object boundary are used as a measure of discontinuity to guide segmentation decisions (Bomans *et al*., 1990). Three approaches using this method are edge detection, deformable templates, and active contours (McInerney and Terzopoulos, 1996; Ji and Yan, 2002; Abd-Almageed *et al*., 2004). In region-based methods, BMS is based on the identification of a homogenous feature which represents one of the brain tissues (Heinonen *et al*., 1998). The hybrid methods use a combination of similarity and discontinuity to segment the images. In all the three BMS approaches, pixels are assigned class labels based on a given criterion.

Due to uncertainty of the brain MRI pixels, using rigid criteria can potentially limit the effectiveness of the technique. For this reason, researchers have developed fuzzy approaches which consider ambiguous regions of an image as fuzzy sets. Using this strategy, each pixel may potentially be assigned to multiple tissue classes. Fuzzy segmentation provides more information than other crisp methods (Wang *et al*., 2008).

Fuzzy c-mean (FCM) is one of the most prominent techniques among the different fuzzy approaches used in BMS (Brandt *et al*., 1994; Yoon *et al*., 1999; Liew and Yan, 2003; Zhang and Chen, 2004; Shen *et al*., 2005; Siyal and Yu, 2005; Chuang *et al*., 2006; Ji *et al*., 2011). There has been extensive research that considers how to use FCM optimization to achieve better results. An adaptive FCM approach was suggested in Pham and Prince (1999a) to estimate INU by multiplying a distance function and clustering centers. This method was generalized for 3D images in Pham and Prince (1999b). A regulative term was proposed in FCM in which spatial information was used to overcome noise effects (Ahmed *et al*., 2002).

Generally, in combination methodology classification tasks involve multisource data fusion and evidential reasoning to achieve higher classification accuracy and robustness. The information extracted from any source in favor of, or against, a given class assignment must be combined with that of other sources to infer the likelihood of this assignment (Binaghi and Madella, 1999). This issue (advantage of data fusion) is also valid when we consider image segmentation as a classification task. Awate *et al*. (2008) proposed a method for brain-tissue segmentation in which the information in structural MRI and

diffusion tensor (DT) images is fused in a statistical framework.

Dempster-Shafer theory (DST) is considered one of the main tools in information fusion research. This theory is a general extension of the Bayesian theory which offers a number of advantages when compared to traditional Bayesian theory (Yager *et al*., 1994). DST can robustly deal with incomplete information and is therefore widely applied in image processing and pattern recognition research (Rakar *et al*., 1999; Lin, 2010; Valente, 2010; Tabassian *et al*., 2011; 2012). Hasanzadeh and Kasaei (2007) proposed a multispectral BMS based on data fusion in which a genetic fuzzy system and DST are used for fuzzy modeling and fusing the results, respectively. In this multispectral BMS approach the results of individual classifiers are applied to three well-known modalities, T1, T2, and PD, and are combined by using DST. Note that these modalities are not recorded in the same coordinate system in real data acquisition. As a result, the performance of the technique is highly dependent on the quality of the data and the algorithm used for registering the images. The other weakness of this method is that it does not use any spatial information, which reduces its accuracy.

In this paper we propose a data fusion approach for BMS based on the application of FCM on different features, and employ DST (evidence theory) to combine evidence obtained through the application of different techniques. The proposed method uses only one of the mentioned modalities (T1-weighted brain MR images), which is applicable on both simulated and real data. Pixel intensity and spatial information are also used. Moreover, a novel mapping is suggested to transform each FCM output to belief structure with particular focal elements. As FCM and DST have the capability to overcome uncertainty, the proposed method would be able to achieve higher accuracy and robustness in BMS.

This work is the extension of our previous work (Ghasemi *et al.*, 2011), including expanded discussions and more experimental results.

2 Basic concepts

2.1 Fuzzy c-mean (FCM)

In FCM, as a development of the hard *K*-means algorithm, every input value will be assigned to all existing clusters (Bezdek, 1981). Pattern membership of a class is based on the similarity of the pattern to the class with respect to all classes. The objective function of the standard FCM which segments an image to c clusters can be defined as

$$J_q(\boldsymbol{u},\boldsymbol{v})=\sum_{i=1}^{c}\sum_{j=1}^{n}u_{ij}^{q}d^2(\boldsymbol{x}_j,\boldsymbol{v}_i)$$
$$\text{subject to } \sum_{i=1}^{c}u_{ij}=1,\ u_{ij}\in[0,\ 1], \tag{1}$$

in which $\boldsymbol{X}=(\boldsymbol{x}_1, \boldsymbol{x}_2, \ldots, \boldsymbol{x}_n)$ is a $p\times n$ data matrix, p is the length of the feature vector $\boldsymbol{x}_j$, and n is the number of feature vectors. In BMS, p=1 (intensity value), n is the number of image pixels, and q is the fuzziness index (in this study, q is 2). u_{ij} is the membership of the jth pattern in the ith cluster, and $\boldsymbol{v}_i$ is the center of the ith fuzzy cluster. d represents the similarity of the feature vector $\boldsymbol{x}_j$ to cluster center $\boldsymbol{v}_i$ in the feature space, which can be calculated with the Euclidean norm as

$$d^2(\boldsymbol{x}_j,\boldsymbol{v}_j)=\left\|\boldsymbol{x}_j-\boldsymbol{v}_j\right\|^2. \tag{2}$$

To minimize the objective function, higher membership values should be assigned to patterns that are close to cluster centers, and lower values assigned to patterns far from cluster centers. By applying derivation of J_q with respect to $\boldsymbol{u}$ and $\boldsymbol{v}$, then setting this derivative equal to zero, the conditions to minimize the objective function (J_q) are

$$u_{ij}=\left(\sum_{k=1}^{c}\left(\frac{d(\boldsymbol{x}_j,\boldsymbol{v}_i)}{d(\boldsymbol{x}_j,\boldsymbol{v}_k)}\right)^{2/(q-1)}\right)^{-1}, \tag{3}$$

$$\boldsymbol{v}_i=\sum_{j=1}^{n}u_{ij}^{q}\boldsymbol{x}_j\Big/\sum_{j=1}^{n}u_{ij}^{q}. \tag{4}$$

According to Eqs. (3) and (4), the patterns are assigned to all existing clusters with associated membership values (MVs), and then new cluster centers are calculated.

The FCM algorithm reaches a solution by an iterative process until a termination criterion is met, i.e., $\|\boldsymbol{v}(t)-\boldsymbol{v}(t-1)\|<\varepsilon$. Finally, by assigning the pattern to a cluster with the highest membership value, a segmentation of the data can be done.

2.2 Dempster-Shafer theory (DST)

DST, also called evidence theory, is a formal framework that provides techniques to characterize evidence based on information from all available evidence. It combines evidence weights from different sources to form new evidence weights.

Assume f is a variable in the domain set Ω. Note that f may also be treated as a question or proposition and Ω as a set of propositions or mutually exclusive and exhaustive hypotheses or answers (Yager *et al*., 1994). In DST, Ω is called the 'frame of discernment' which is denoted as $\Omega=\{C_1, C_2, \ldots, C_n\}$. DST is essentially a generalized Bayesian statistical theory (Shafer, 1976). For instance, probabilities in the Bayesian approach can be assigned only to the singleton subsets (i.e., elements) of Ω but in DST they are assigned to all subsets of Ω.

In DST a mass function μ is defined as a mapping from the power set Ω in the unit interval [0, 1] called basic belief assignment (BBA), where μ: $2^{\Omega}\rightarrow[0, 1]$, $\mu(\varnothing)=0$, and $\sum_{A\subseteq\Omega}\mu(A)=1$. The notation 2^{Ω} relates to the power set of Ω. The value $\mu_i(A)$ is interpreted as a fraction of belief that is committed to A for the available evidence i (Beynon *et al*., 2001). Focal elements are sets that receive a non-null mass value.

It is attractive to overcome the restriction of conventional probability theory by representation of both imprecision and uncertainty through the definition of two functions, plausibility (Pls) and belief (Bel), both derived from a mass function μ (Shafer, 1976). The measures of belief and plausibility for A are determined as follows:

$$\mathrm{Bel}(A)=\begin{cases}\sum_{B\subset A}\mu(B), & \forall A\subseteq\Omega, A\neq\varnothing,\\ 0, & A=\varnothing,\end{cases} \tag{5}$$

$$\mathrm{Pls}(A)=\begin{cases}\sum_{B\cap A\neq\varnothing}\mu(B), & \forall A\subseteq\Omega, A\neq\varnothing,\\ 0, & A=\varnothing.\end{cases} \tag{6}$$

Bel(A) represents the confidence that a proposition f lies in A or any subset of A. Clearly Pls(A) represents the extent to which we fail to disbelieve A (Beynon *et al*., 2001). DST provides an explicit measure of ignorance about event A and its complementary $\bar{A}$ as length of the interval [Bel(A), Pls(A)], called the belief interval. It can also be interpreted as a measure of imprecision of the 'true probability' of A (Bloch, 1996).

One of the main advantages of DST is the flexible combination operator it uses to combine information according to Dempster's rule of combination. Suppose that μ_1 and μ_2 are two independent belief structures on a frame of discernment Ω, with focal elements Ψ_i (i=1, 2, …, n_1) and Ψ_j (j=1, 2, …, n_2). The combination of μ_1 and μ_2 (also called the joint mass, $\mu_{1,2}$) is defined as

$$\mu_1\oplus\mu_2(\zeta_k)=\mu_{1,2}(\zeta_k)=\frac{\sum_{\Psi_i\cap\Psi_j=\zeta_k}\mu_1(\Psi_i)\mu_2(\Psi_j)}{1-\sum_{\Psi_i\cap\Psi_j=\varnothing}\mu_1(\Psi_i)\mu_2(\Psi_j)}, \tag{7}$$

where $\mu_{1,2}$ is another BBA whose focal element is $\zeta_k=\Psi_i\cap\Psi_j$. Dempster's rule is both commutative and associative (Yager *et al*., 1994).

2.3 Singular value decomposition (SVD)

SVD is an important tool used in digital signal and statistical data processing (Ghasemi and Karami Mollaei, 2009; Afzalian *et al*., 2010). Applying SVD on a typical $\boldsymbol{X}_{m\times n}$ matrix yields

$$\boldsymbol{X}=\boldsymbol{U}\boldsymbol{\Sigma}\boldsymbol{V}^{\mathrm{T}}, \tag{8}$$

where $\boldsymbol{U}_{m\times m}$ and $\boldsymbol{V}_{n\times n}$ are singular vector matrices and $\boldsymbol{\Sigma}_{m\times n}$ is a diagonal matrix with rank r. The diagonal entries of $\boldsymbol{\Sigma}$ ($\sigma_{11}>\sigma_{22}>\ldots>\sigma_{rr}>0$) are equal to the singular values of $\boldsymbol{X}$. In fact, these singular values contain some information about signal energy. In the process of reconstructing $\boldsymbol{X}$, higher singular values are more effective.

3 The proposed method

As mentioned above, the main problem in brain MRI segmentation is intensity uncertainty, and this difficulty motivates the development of fuzzy approaches. FCM is one of the commonly used tools among different fuzzy approaches used for BMS.

Reasonable results are expected when each pattern is assigned to a cluster with the highest MV in the final stage of the FCM algorithm (Section 2.1). However, when the pattern MVs are too close to each

other, the selection of one of the clusters may lead to unreasonable results.

In this paper, an information fusion strategy based on DST is presented. This approach considers spatial information and interprets FCM results for brain MRI segmentation. The main idea of the proposed method is that undesirable artifact effects are shown in different FCM outputs. These artifact effects become smaller by using DST. Since the proposed method combines the FCM results using DST, we refer to our method as FCMDS.

Fig. 2 shows the block diagram depicting the FCMDS method. FCMDS extracts three features from the original images, and considers spatial information (Section 3.1). In the next stage of FCMDS, FCMs are used for clustering. In this stage the clustering process is applied to each extracted feature independently. The outputs of FCM are interpreted as BBA. Finally, these computed BBAs are combined using DST.

3.1 Feature set

The three features considered in this analysis are pixel intensity and both mean and largest singular values of neighborhood pixels. It is clear that pixel intensity contains crucial information and is the most important feature of BMS. For calculation of both mean and largest singular values (Fig. 3), a 3×3 matrix around the prototype pixel is considered.

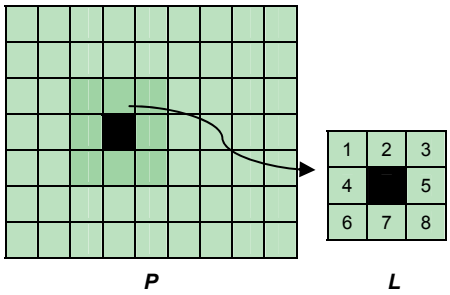

Fig. 3 Original picture (*P*) and a 3×3 matrix around the prototype pixel (*L*)

Mean and largest singular values (spatial information) are defined for each 3×3 matrix based on Eqs. (9) and (10). We have

$$F_2 = \frac{1}{n}\sum_{i=1}^{n} \boldsymbol{X}_i = E(\boldsymbol{X}), \tag{9}$$

where $\boldsymbol{X}_i$ is the neighborhood pixel value, n=8 is the number of pixels, and $E(\boldsymbol{X})$ is the mean value. The largest singular value can be calculated as

$$\mathrm{SVD}(\boldsymbol{L}) = \boldsymbol{U}\begin{bmatrix} \sigma_{11} & 0 & 0 \\ 0 & \sigma_{22} & 0 \\ 0 & 0 & \sigma_{33} \end{bmatrix}\boldsymbol{V}^{\mathrm{T}} \Rightarrow F_3 = \sigma_{11}, \tag{10}$$

where σ_{11} is the largest singular value of $\boldsymbol{L}$, and

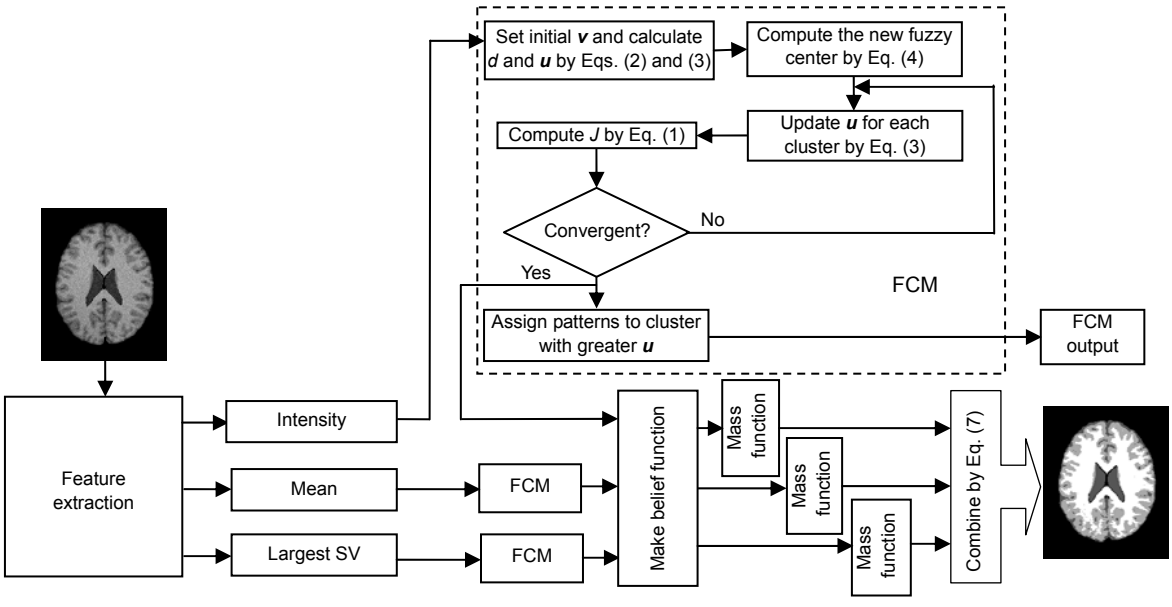

Fig. 2 Block diagram of the proposed method FCMDS which combines FCM results using Dempster-Shafer theory

contains significant information about the matrix and can be used as an important feature in BMS. Mean and largest singular value features contain information about the bias of the neighborhood pixels and the energy of the crucial eigenvector, respectively.

3.2 Construction of belief structure

In the normal brain MRI, f is one of the extracted features whose frame of discernment is $\Omega=\{W, G, C\}$. Therefore, the power set of Ω is $\boldsymbol{R}=[\{W\}, \{G\}, \{C\}, \{W, G\}, \{W, C\}, \{G, C\}, \{W, G, C\}]$. W, G, and C symbolize white matter, gray matter, and cerebrospinal fluid, respectively. The BBAs assigned to atomic members (the first three elements) of $\boldsymbol{R}$ are deterministic while the BBAs assigned to other elements of $\boldsymbol{R}$ include uncertainty. The ultimate goal of data fusion is the reduction of uncertainty.

In FCMDS, when the FCM algorithm reaches a solution, the MVs assigned to tissues for every pixel are used to build the BBAs. This process applies for each feature separately. For this purpose, the three ratios of the available MV assignment obtained from FCM which are also greater than one are calculated, and these three situations will be considered as no-uncertainty (NU), semi-uncertainty (SU), and perfect-uncertainty (PU). Note that in this study, the term 'RMV' refers to the ratio of MVs that are greater than one. For description of the above mentioned situations, two thresholds α and β are selected as α=1.5 and β=3. β controls the boundary between NU and SU while α controls the boundary between SU and PU. A more detailed explanation of these three situations is given below.

3.2.1 No-uncertainty (NU)

NU is a situation in which the RMV is greater than β. Consider a prototype pixel where the FCM gives u_W=0.18 and u_G=0.81. The RMV is 0.81/0.18=4.5>β. Thus, the two MVs fall in the NU category. Based on the final stage of FCM, the pixel must be assigned to GM. Due to the large difference between the two available MVs, this decision has high credibility. In NU all the MVs are interpreted as BBA without the need for any further change. In another word, MVs map to singleton subsets of $\boldsymbol{R}$. When all three RMVs are in the NU category, the focal element has three atomic factors, denoted as $\boldsymbol{R}=[\{W\}, \{G\}, \{C\}]$, where their BBAs are FCM MVs.

3.2.2 Semi-uncertainty (SU)

In SU at least one of the RMVs falls between the two thresholds. Suppose that for a prototype pixel the FCM gives u_W=0.25 and u_G=0.65. The RMV is then α<0.65/0.25=2.6<β, and consequently the two mentioned MVs are in the SU category. Assigning the specified pixel to GM may be incorrect, because u_W is large enough; therefore, FCM may fail. A measure of distance uncertainty can be used to generate belief structures as a basis to overcome the mentioned drawback. In fact, in this case the uncertainty is transferred to a mutual belief structure and this uncertainty is controlled by DST. We define the uncertainty distance λ as $\lambda_{WG}=|u_W-u_G|/(\beta-\alpha)$. Then for making the belief structures, the BBAs are calculated using $\mu\{W\}=u_W-\lambda_{WG}/2$, $\mu\{G\}=u_G-\lambda_{WG}/2$, $\mu\{W, G\}=\lambda_{WG}$. The value of λ depends on the two selected thresholds and the assigned MVs. Furthermore, when constructing the BBA, $\lambda/2$ is chosen from each primary MV and used to build the mutual mass value, which is equivalent to the situation in which there are no other usable sources of information. When making decisions in such a situation, all mutual mass values are equally divided between the atomic focal elements.

It is possible that more than one of the RMVs falls between two selected thresholds. In such a situation, a new formulation is needed to generalize the previous formulation. Suppose that all the three RMVs are in SU. In this situation the uncertainty distances are $\lambda_{WG}=|u_W-u_G|/(\beta-\alpha)$, $\lambda_{WC}=|u_W-u_C|/(\beta-\alpha)$, and $\lambda_{GC}=|u_G-u_C|/(\beta-\alpha)$. Then the BBAs are calculated as

$$\begin{cases} \mu\{W\}=u_W-\dfrac{3}{4}(\lambda_{WG}+\lambda_{WC}), \\ \mu\{G\}=u_G-\dfrac{3}{4}(\lambda_{WG}+\lambda_{GC}), \\ \mu\{C\}=u_C-\dfrac{3}{4}(\lambda_{WC}+\lambda_{GC}), \\ \mu\{W,G\}=\lambda_{WG},\ \mu\{W,C\}=\lambda_{WC},\ \mu\{G,C\}=\lambda_{GC}, \\ \mu\{W,G,C\}=\dfrac{1}{2}(\lambda_{WG}+\lambda_{WC}+\lambda_{GC}). \end{cases} \tag{11}$$

From the above formulation, we see that the focal elements are the power set of the frame of discernment without the null set.

3.2.3 Perfect-uncertainty (PU)

PU is a critical situation in which the RMVs are smaller than α. Assume that for a prototype pixel the FCM values are u_W=0.45 and u_G=0.55. The RMV is then 0.55/0.45=1.22<α, and is therefore in PU. If there is no additional source of information, this pixel will be assigned to GM. Since the MVs used to assign the pixel to WM and GM are close to each other, this decision is subjective and may be inaccurate; in other words, in this case the FCM may fail. As mentioned, in PU the appropriate distance between available MVs cannot be found, and in such a situation, the BBAs are calculated as $\mu\{W\}=\mu\{G\}=\mu\{W, G\}=(u_W+u_G)/3$. The proposed formulation demonstrates that the larger part of MV has been deposited to non-atomic focal elements rather than SU. Since such focal elements can contain uncertainty, the mentioned drawback is solved systematically by DST.

If more than one RMV is smaller than α, a new formulation is needed to generalize the earlier formulation. Suppose that all three RMVs are in PU. In this situation the BBAs are calculated according to the following steps:

1. Consider 2^{Ω} without the null set as the set of focal elements. The elements of the set are

$$\{W\},\ \{G\},\ \{C\},\ \{W, G\},\ \{W, C\},\ \{G, C\},\ \{W, G, C\}. \tag{12}$$

2. Calculate N as the number of repetitions in any class (in the three-class problem according to expression (12), N is 4).

3. Allocate the same division of any u_i (u_i/N, $i=W, G, C$) to those focal elements that contain the ith class.

$$\begin{cases} \mu\{W\}=\dfrac{u_W}{4},\ \mu\{G\}=\dfrac{u_G}{4},\ \mu\{C\}=\dfrac{u_C}{4}, \\ \mu\{W,G\}=\dfrac{u_W}{4}+\dfrac{u_G}{4},\ \mu\{W,C\}=\dfrac{u_W}{4}+\dfrac{u_C}{4}, \\ \mu\{G,C\}=\dfrac{u_G}{4}+\dfrac{u_C}{4},\ \mu\{W,G,C\}=\dfrac{u_W}{4}+\dfrac{u_G}{4}+\dfrac{u_C}{4}. \end{cases} \tag{13}$$

3.2.4 Applicability of FCMDS for other problems

In this study the problem of normal BMS with three classes is studied. In other words, FCM has three MVs and there are three RMVs. Consequently, the aforementioned formulations are sufficient. In this subsection the applicability of the proposed method is considered for problems with four or more classes.

To extend the proposed strategy to a problem with more than three classes, a four-class problem is considered where the MVs satisfy $u_1<u_2<u_3<u_4$. As mentioned above, NU is a situation in which all available MVs are converted to BBA without any further change, so no problems arise when we extend this situation to a problem with more than three classes. Suppose all the RMVs are in the SU category. Therefore we have

$$\alpha \le u_{i+1}/u_i \le \beta, \quad i=1, 2, 3. \tag{14}$$

Using the left-hand boundary (critical) condition of Eq. (14) with α=1.5, the ratio between u_4 and u_1 is obtained as follows:

$$\frac{u_4}{u_1}=\frac{u_4}{u_3}\frac{u_3}{u_2}\frac{u_2}{u_1}=\alpha^3=3.375>\beta. \tag{15}$$

Eq. (15) contradicts the last assumption (all the RMVs are in the SU category), because one of the RMVs is greater than β; in other words, two MVs (u_1 and u_4) are in the NU category. None of the RMVs can fall between these two thresholds. Therefore, in the problem with four or more classes, two or three RMVs can fall between two thresholds, as explained in Section 3.2.2. The extension of PU to the problem with four or more classes is straightforward, and can be done in the three steps described in Section 3.2.3.

4 Discussions about uncertainty decrement in the three-element problem by DST

In this section, the uncertainty decrement in DST-based three-element pattern recognition is discussed. Assume that for a given problem the frame of discernment is $\Omega=\{C_1, C_2, C_3\}$, in which two pieces of evidence A and B have the following belief structures:

Focal element	Evidence A	Evidence B
$\mu\{C_1\}$	a	h
$\mu\{C_2\}$	b	i
$\mu\{C_3\}$	c	j
$\mu\{C_1, C_2\}$	d	k
$\mu\{C_1, C_3\}$	e	l
$\mu\{C_2, C_3\}$	f	m
$\mu\{C_1, C_2, C_3\}$	g	n

By combining two beliefs using DST, the non-normalized joint masses are given by

$$\mu_{AB}\{\varnothing\}=h(b+c+f)+i(a+c+e)+j(a+b+d)+kc+lb+ma,$$
$$\mu_{AB}\{C_1\}=a(h+k+l+n)+d(h+l)+e(h+k)+gh,$$
$$\mu_{AB}\{C_2\}=b(i+k+m+n)+d(m+i)+f(i+k)+gi,$$
$$\mu_{AB}\{C_3\}=c(j+l+m+n)+e(j+m)+f(j+l)+gj,$$
$$\mu_{AB}\{C_1, C_2\}=dk+dn+gk,\ \mu_{AB}\{C_1, C_3\}=el+en+lg,$$
$$\mu_{AB}\{C_2, C_3\}=fm+fn+gm,\ \mu_{AB}\{C_1, C_2, C_3\}=gn.$$

It is clear that the uncertainty terms related to the beliefs of A and B are $d+e+f+g$ and $k+l+m+n$, respectively. Also, the normalized uncertainty term for the combination of two beliefs can be written as

$$\begin{aligned}&(\mu_{AB}\{C_1,C_2\}+\mu_{AB}\{C_1,C_3\}+\mu_{AB}\{C_2,C_3\}\\&+\mu_{AB}\{C_1,C_2,C_3\})/(1-\mu_{AB}(\varnothing))\\&=(dk+dn+gk+el+en+lg+fm\\&+fn+gm+gn)/(1-\mu_{AB}(\varnothing))\\&=d\frac{k+n}{1-\mu_{AB}(\varnothing)}+e\frac{l+n}{1-\mu_{AB}(\varnothing)}\\&+g\frac{k+l+n+m}{1-\mu_{AB}(\varnothing)}+f\frac{m+n}{1-\mu_{AB}(\varnothing)}.\end{aligned}\tag{16}$$

To find the conditions in which the uncertainty of the combined beliefs is lower than the uncertainty of an individual belief (e.g., evidence A), consider

$$\begin{aligned}d+e+f+g>{}&d\frac{k+n}{1-\mu_{AB}(\varnothing)}+e\frac{l+n}{1-\mu_{AB}(\varnothing)}\\&+g\frac{k+l+n+m}{1-\mu_{AB}(\varnothing)}+f\frac{m+n}{1-\mu_{AB}(\varnothing)}.\end{aligned}\tag{17}$$

On the left-hand side of inequality (17), the coefficients of each BBA (d, e, f, and g) are equal to one, but on the right-hand side, all of BBAs have coefficients not equal to one. Note that $\frac{k+l+n+m}{1-\mu_{AB}(\varnothing)}$ is the largest coefficient. If $\frac{k+l+n+m}{1-\mu_{AB}(\varnothing)}\le 1$, then all of the other coefficients on the right-hand side are lower than one and thus inequality (17) is valid.

$$\frac{k+l+n+m}{1-\mu_{AB}(\varnothing)}\le 1\Rightarrow k+l+n+m\le 1-\mu_{AB}(\varnothing).\tag{18}$$

Since the sum of all BBAs is equal to one, we have

$$k+l+m+n=1-(h+i+j).\tag{19}$$

Substituting Eq. (19) into Eq. (18), the following condition is achieved:

$$h+i+j\ge\mu_{AB}(\varnothing).\tag{20}$$

The same scenario is valid for other evidence (e.g., evidence B), which leads to the following condition:

$$a+b+c\ge\mu_{AB}(\varnothing).\tag{21}$$

Accordingly, if the sum of certainty terms of belief of evidence (e.g., B or A) is equal to or greater than the null mass of the combination of two beliefs, then the uncertainty of the combined belief is always lower than the uncertainty of any other belief of the evidence (e.g., A or B). Therefore, the uncertainty of combined beliefs decreases systematically.

5 Experimental results

In the data fusion part of the proposed algorithm, the information from different sources is combined using Dempster's rule of combination to generate robust results. To generate the fused data using Eq. (7), each FCM with a single extracted feature is considered independently as an evidence source. The proposed method was tested on two publicly available datasets. The first dataset contains simulated MR images and is available on the Brainweb (http://www.bic.mni.mcgill.ca/brainweb). The second dataset contains real MR images obtained from the Internet Brain Segmentation Repository (IBSR) (http://www.cma.mgh.harvard.edu/ibsr). Extra non-brain tissues are removed from these brain images prior to segmentation. The proposed algorithm is compared with the FCM, BCFCM (Ahmed *et al*., 2002), LNLFCM (Wang *et al*., 2008), SPM5, FAST, LOCUS-T, and FBM-T (Scherrer *et al*., 2010) methods when applied to the simulated dataset. The real data was used to compare the proposed method with CSWTSOM, SPM5, and FAST which were reported in Tsang *et al*. (2008) and Demirhan and Güler (2011). In FCM the intensity of the pixels is used as a feature, whereas in

BCFCM all parameters are selected, as reported in Ahmed *et al*. (2002). The chosen parameter values for LNLFCM are: a standard deviation of 30 associated with the Gaussian kernel, a degree of filtering of 1000, a window size of 3 for the neighborhood, and a weight of 7 for all pixels in the window of searching (Wang *et al*., 2008). The results of the other methods were reported in Scherrer *et al*. (2010) and Demirhan and Güler (2011). In all experiments the two thresholds α and β were selected as 1.5 and 3, respectively.

5.1 Evaluation criteria

Different criteria have been used to evaluate the segmentation performance quantitatively and to compare the different approaches. The evaluation criteria are Dice similarity and Accuracy, given by

$$\text{Dice}=\frac{2\left|A_i\cap B_i\right|}{\left|A_i\right|+\left|B_i\right|}=\frac{2\times\text{TP}}{2\times\text{TP}+\text{FP}+\text{FN}}, \tag{22}$$

$$\text{Accuracy}=\frac{\text{TP}+\text{TN}}{\text{TP}+\text{TN}+\text{FP}+\text{FN}}, \tag{23}$$

where A_i and B_i are the reference and result sets of segmented pixels, respectively, and $|A_i|$ is the number of pixels in A_i (Ahmed *et al*., 2002). In Eqs. (22) and (23), TP, TN, FP, and FN are defined as true positive, true negative, false positive, and false negative, respectively (Hadjiprocopis *et al*., 2005). Large values for each of the two metrics indicate better segmentation.

5.2 Simulated brain MRI

Brainweb provides simulated brain datasets which contain a set of realistic MRIs created using an MRI simulator (Wang *et al*., 2008). In this subsection, T1-weighted brain MR images with a slice thickness of 1 mm and a volume size of 217×181×181 are employed to investigate the proposed method. These images are obtained from the Brainweb Simulated Brain Database at the McConnell Brain Imaging Centre of the Montreal Neurological Institute (MNI), McGill University.

Fig. 4a shows a slice of the simulated 3D volume of an MRI with 9% Rician noise and 40% INU (slice=96). The ground truth of this image is shown in Fig. 4b. Segmentation results of FCM, BCFCM, and LNLFCM are shown in Figs. 4c, 4d, and 4e, respectively. The result of the proposed method is shown in Fig. 4f.

As shown in Figs. 4c and 4d, the standard FCM and BCFCM are extremely influenced by the artifacts. On the other hand, the comparison of results shown in Figs. 4b and 4e shows that the GM diameter is greater than the ground truth for the LNLFCM approach. However, FCMDS can generally reduce the effects of the image noise and INU. Dice similarity and Accuracy indices of Fig. 4 are shown in Table 1.

According to Table 1 and Fig. 4, FCMDS performs well when compared to the other methods. Note that to evaluate the effectiveness of a segmentation method in each tissue, the key quantitative

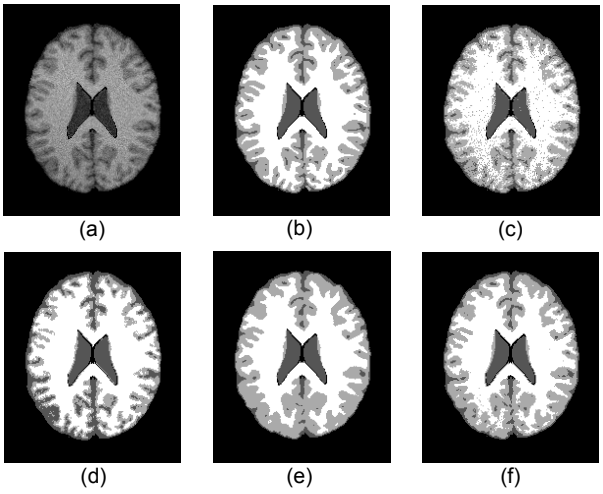

Fig. 4 Comparison of the segmentation results on a simulated brain MR image

(a) Original image with 9% noise and 40% INU (slice=96); (b) Ground truth; (c) FCM segmentation result; (d) BCFCM segmentation result; (e) LNLFCM segmentation result; (f) FCMDS segmentation result

Table 1 Dice and Accuracy for different methods in Fig. 4

Method	Dice			Accuracy		
	CSF	GM	WM	CSF	GM	WM
FCM	0.897	0.826	0.897	0.967	0.871	0.904
BCFCM	0.777	0.724	0.918	0.918	0.833	0.915
LNLFCM	0.890	0.882	0.932	0.968	0.911	0.935
FCMDS	0.932	0.890	0.936	0.979	0.918	0.938

CSF: cerebro-spinal fluid; GM: gray matter; WM: white matter

criteria should be considered in conjunction with the associated image. We further analyze the performance of the proposed algorithm for different artifacts. Figs. 5a, 5g, and 5m are simulated MR images without INU and with noise levels 7%, 5%, and 3%, respectively. Figs. 5b, 5h, and 5n show the ground truths of the corresponding noisy images. Our algorithm results are shown in Figs. 5f, 5l, and 5r.

Fig. 5 shows clearly that FCMDS performs better than the other methods. In general, the images taken near the base of the brain (Fig. 5a) and near the top of the skull (Fig. 5m) are more difficult to segment (Wang *et al*., 2008). Figs. 5f and 5r show that we can achieve good results using FCMDS.

Table 2 gives the mean Dice and Accuracy indices of Fig. 5. According to Table 2, FCM performs better than FCMDS when the noise levels are low (slice=130 and 3% noise), but when the noise level increases, FCM is inferior to FCMDS. In other words, FCMDS is more robust. To further investigate the robustness of the method, we implemented FCM and FCMDS in the 3D space and applied these methods on the simulated MRI with various noise levels and 20% non-uniformity. Table 3 shows the segmentation results for each tissue separately.

According to Table 3, we can see that FCMDS produces more accurate segmentation than FCM. The mean and variance of the results show that FCMDS is very robust when dealing with artifacts.

In the final evaluation using the Brainweb dataset, Table 4 shows the comparison of our method with SPM5, FAST, LOCUS-T, and FBM-T over eight experiments for different noise levels (3%, 5%, 7%, 9%) and non-uniformities (20%, 40%).

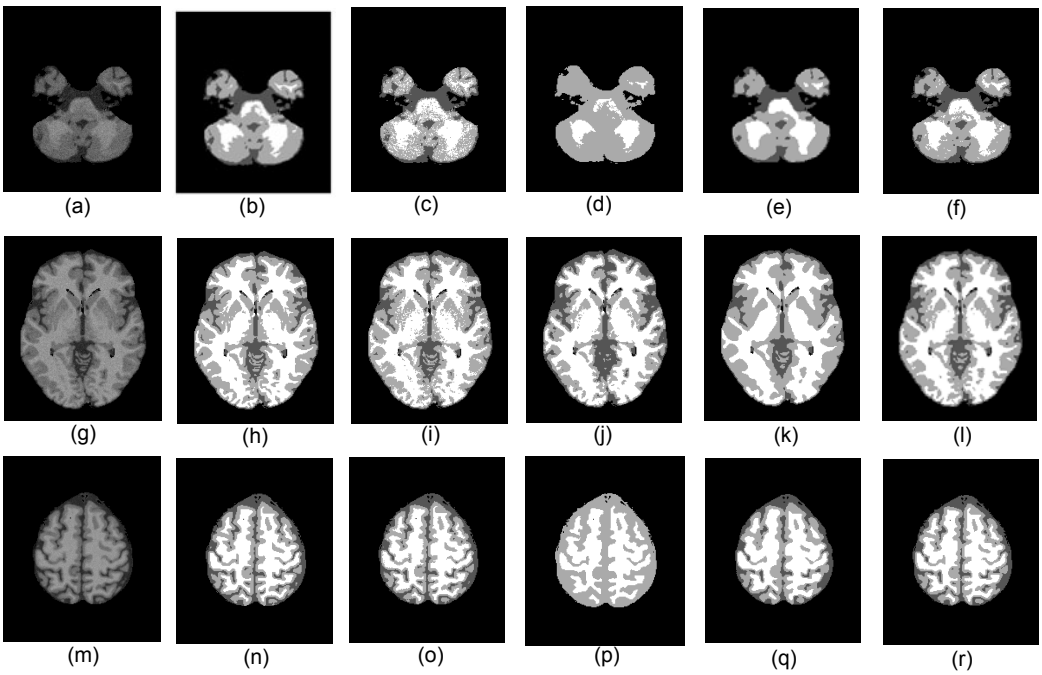

Fig. 5 Comparison of the segmentation results on a simulated brain MR image

(a, g, m) Original images with 7%, 5%, and 3% noises (slice=30, 70, 130, respectively); (b, h, n) Ground truth; (c, i, o) FCM segmentation result; (d, j p) BCFCM segmentation result; (e, k, q) LNLFCM segmentation result; (f, l, r) FCMDS segmentation result

Table 2 Mean Dice and mean Accuracy for different methods in Fig. 5

Method	Mean Dice			Mean Accuracy		
	Slice=30	Slice=70	Slice=130	Slice=30	Slice=70	Slice=130
FCM	0.838	0.933	0.965	0.897	0.952	0.976
BCFCM	0.550	0.834	0.532	0.794	0.889	0.791
LNLFCM	0.901	0.904	0.900	0.942	0.953	0.932
FCMDS	0.907	0.936	0.952	0.943	0.979	0.967

Table 3 Comparison of Dice and Accuracy of FCM and FCMDS applied on 3D MRI

Noise	Dice similarity						Accuracy					
	WM		GM		CSF		WM		GM		CSF	
	FCM	FCMDS	FCM	FCMDS	FCM	FCMDS	FCM	FCMDS	FCM	FCMDS	FCM	FCMDS
1%	0.977	0.950	0.970	0.941	0.973	0.952	0.991	0.981	0.972	0.947	0.981	0.965
3%	0.966	0.948	0.949	0.935	0.953	0.946	0.987	0.981	0.954	0.942	0.967	0.961
5%	0.950	0.944	0.912	0.926	0.922	0.937	0.981	0.980	0.925	0.933	0.944	0.954
7%	0.928	0.937	0.869	0.911	0.878	0.922	0.972	0.976	0.883	0.920	0.911	0.944
9%	0.898	0.929	0.822	0.898	0.836	0.911	0.960	0.973	0.842	0.901	0.881	0.935
Ave.	0.944	0.942	0.904	0.922	0.912	0.934	0.978	0.978	0.915	0.929	0.937	0.952
Var.	0.0010	0.0001	0.0036	0.0003	0.0031	0.0003	0.0001	0.0000	0.0028	0.0003	0.0017	0.0002

CSF: cerebro-spinal fluid; GM: gray matter; WM: white matter

Table 4 Mean Dice similarity index of different methods for different values of noise (3%, 5%, 7%, 9%) and non-uniformity (20%, 40%)

Method	Mean Dice			Ave.	Var.
	WM	GM	CSF		
SPM5	0.936	0.916	0.799	0.884	0.0055
FAST	0.937	0.918	0.798	0.884	0.0057
LOCUS-T	0.904	0.892	0.795	0.864	0.0036
FBM-T	0.941	0.913	0.796	0.883	0.0059
FCMDS	0.927	0.911	0.920	0.919	0.0001

CSF: cerebro-spinal fluid; GM: gray matter; WM: white matter

As seen in Table 4, FCMDS has results comparable to those obtained using SPM5, FAST, LOCUS-T, and FBM-T for both WM and GM tissues, but it is better able to identify the CSF tissue. This CSF tissue identification leads to an improved average (Ave.) and variance (Var.) for FCMDS. This comparison demonstrates the high performance and robustness of the proposed method.

5.3 Real brain MRI

The proposed algorithm was also evaluated using real MR images. The 20 normal MR brain data sets and their manual segmentations were provided by the Center for Morphometric Analysis at Massachusetts General Hospital and are available at http://www.cma.mgh.harvard.edu/ibsr.

Figs. 6a and 6b show a real T1-weighted normal MR image (IBSR 205_3) and its manually segmented images as provided by the Web, respectively. Fig. 6c shows the output of our proposed algorithm, which leads to satisfactory results. The Dice similarities of WM and GM of each image slice are shown in Fig. 7.

The mean Dice similarity values for WM and GM achieved by our proposed algorithm in this volume were 0.743 and 0.853, respectively.

(a) (b) (c)

Fig. 6 T1-weighted real brain MRI from IBSR (slice=25)
(a) Original MR image; (b) Manual segmentation result; (c) FCMDS segmentation result

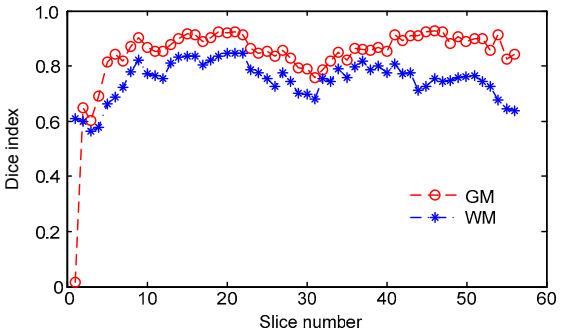

Fig. 7 Dice similarity index of each slice in real brain MRI

FCMDS was implemented for 10 of the 20 available datasets and the corresponding Dice similarity values are given in Table 5. We also give the results obtained using the CSWTSOM approach (Demirhan and Güler, 2011). Demirhan and Güler (2011) applied CSWTSOM to 10 out of 20 available data sets and therefore we used the same 10 data sets for comparison.

According to Table 5, FCMDS produces acceptable results for 3D MRI datasets and performs better than CSWTSOM with respect to WM and GM identification.

As a final evaluation, FCMDS was applied to all the 20 normal MR brain data sets from IBSR, and the Dice similarities were compared with those obtained

from the application of the SPM5 and FAST methods (Table 6).

Table 5 Comparison of the Dice index of CSWTSOM and FCMDS for 3D real brain MRI

Dataset	Dice			
	WM		GM	
	CSWTSOM	FCMDS	CSWTSOM	FCMDS
2_4	0.46	0.60	0.62	0.69
5_8	0.72	0.67	0.82	0.77
7_8	0.52	0.73	0.70	0.84
11_3	0.77	0.76	0.82	0.85
13_3	0.75	0.75	0.83	0.85
16_3	0.71	0.67	0.82	0.76
100_23	0.74	0.76	0.84	0.86
111_2	0.79	0.79	0.81	0.84
191_3	0.75	0.86	0.80	0.85
205_3	0.78	0.74	0.83	0.85
Ave.	0.70	0.73	0.79	0.82
Var.	0.0129	0.0028	0.0051	0.0029

GM: gray matter; WM: white matter

Table 6 Average Dice similarity of all the 20 normal brain data sets for SPM5, FAST, and FCMDS

Method	Average Dice similarity*	Var.
SPM5	0.790	0.0050
FAST	0.756	0.1300
FCMDS	0.783	0.0029

* For the whole brain

Given the average Dice similarity index and variance shown in Table 6, FCMDS clearly performs better than FAST and is comparable to SPM5, although FCMDS has a lower variance.

6 Conclusions

In this paper a novel algorithm is proposed for brain MRI segmentation based on fuzzy c-mean and Dempster-Shafer evidence theory. In the proposed method, FCMDS, pixel intensity and spatial information are used as features. In the proposed formulation the uncertainty from the FCM results is mapped to the mutual belief structures in which the generated uncertainty is controlled using Dempster's rules of combination. No-, semi-, and perfect-uncertainty are three situations considered for managing uncertainty. Uncertainty decrement is discussed for the three-element problem. The salient aspect of this work is the interpretation of each FCM output to determine the belief structures with particular focal elements, which leads to our improved results. To verify the practical applicability of such a technique, simulations were performed using both simulated and real datasets. Comparisons of the proposed method to different algorithms show that our method offers a considerable improvement in brain MRI segmentation.

Acknowledgements

We are grateful for the help and support of Jianzhong WANG and Dirk-Jan KROON. We would also like to extend special thanks to the Brainweb Simulated Brain Database at the McConnell Brain Imaging Centre of the Montreal Neurological Institute (MNI), McGill University, and the Center for Morphometric Analysis at Massachusetts General Hospital for providing datasets. Lastly, we would like to thank Kent University and Babol University of Technology for their support.

References

Abd-Almageed, W., El-Osery, A., Smith, C., 2004. A fuzzy-statistical contour model for MRI segmentation and target tracking. *SPIE*, **5438**:25-33. [doi:10.1117/12.541406]

Afzalian, A., Karami Mollaei, M.R., Dousti, M., Ghasemi, J., 2010. A new approach for speech enhancement based on singular value decomposition and wavelet transform. *Aust. J. Basic Appl. Sci.*, **4**(8):3602-3612.

Ahmed, M.N., Yamany, S.M., Mohamed, N., Farag, A.A., Moriarty, T., 2002. A modified fuzzy c-means algorithm for bias field estimation and segmentation of MRI data. *IEEE Trans. Med. Imag.*, **21**(3):193-199. [doi:10.1109/42.996338]

Awate, S.P., Zhang, H., Simon, T.J., Gee, J.C., 2008. Multivariate Segmentation of Brain Tissues by Fusion of MRI and DTI Data. Proc. 5th IEEE Int. Symp. on Biomedical Imaging: from Nano to Macro, p.213-216. [doi:10.1109/ISBI.2008.4540970]

Beynon, M., Cosker, D., Marshall, D., 2001. An expert system for multi-criteria decision making using Dempster Shafer theory. *Expert Syst. Appl.*, **20**(4):357-367. [doi:10.1016/S0957-4174(01)00020-3]

Bezdek, J.C., 1981. Pattern Recognition with Fuzzy Objective Function Algorithms. Plenum Press, New York. [doi:10.1007/978-1-4757-0450-1]

Binaghi, E., Madella, P., 1999. Fuzzy Dempster-Shafer reasoning for rule-based classifiers. *Int. J. Intell. Syst.*, **14**(6):559-583. [doi:10.1002/(SICI)1098-111X(199906)14:6<559::AID-INT2>3.0.CO;2-#]

Bloch, I., 1996. Some aspects of Dempster-Shafer evidence theory for classification of multi-modality medical images taking partial volume effect into account. *Pattern Recogn. Lett.*, **17**(8):905-919. [doi:10.1016/0167-8655(96)00039-6]

Bomans, M., Hohne, K.H., Tiede, U., Riemer, M., 1990. 3-D segmentation of MR images of the head for 3-D display. *IEEE Trans. Med. Imag.*, **9**(2):177-183. [doi:10.1109/42.56342]

Brandt, M.E., Bohan, T.P., Kramer, L.A., Fletcher, J.M., 1994. Estimation of CSF, white and gray matter volumes in hydrocephalic children using fuzzy clustering of MR images. *Comput. Med. Imag. Graph.*, **18**(1):25-34. [doi:10.1016/0895-6111(94)90058-2]

Brechbühler, C., Gerig, G., Székely, G., 1996. Compensation of Spatial Inhomogeneity in MRI Based on a Multi-valued Image Model and a Parametric Bias Estimate. Proc. Visualization in Biomedical Computing, p.141-146. [doi:10.1007/BFb0046948]

Chuang, K.S., Tzeng, H.L., Chen, S., Wu, J., Chen, T.J., 2006. Fuzzy c-means clustering with spatial information for image segmentation. *Comput. Med. Imag. Graph.*, **30**(1):9-15. [doi:10.1016/j.compmedimag.2005.10.001]

Demirhan, A., Güler, I., 2011. Combining stationary wavelet transform and self-organizing maps for brain MR image segmentation. *Eng. Appl. Artif. Intell.*, **24**(2):358-367. [doi:10.1016/j.engappai.2010.09.008]

Ghasemi, J., Karami Mollaei, M.R., 2009. A new approach for speech enhancement based on eigenvalue spectral subtraction. *Signal Process. Int. J.*, **3**(4):34-41.

Ghasemi, J., Karami Mollaei, M.R., Ghaderi, R., Hojjatoleslami, S.A., 2011. Brain Tissue Segmentation by FCM and Dempster-Shafer Theory. 7th Iranian Conf. on Machine Vision and Image Processing, p.1-5. [doi:10.1109/IranianMVIP.2011.6121577]

Gispert, J.D., Reig, S., Pascau, J., Vaquero, J.J., Garcia-Barreno, P., Desco, M., 2004. Method for bias field correction of brain T1-weighted magnetic resonance images minimizing segmentation error. *Human Brain Map.*, **22**(2):133-144. [doi:10.1002/hbm.20013]

Hadjiprocopis, A., Rashid, W., Tofts, P.S., 2005. Unbiased segmentation of diffusion-weighted magnetic resonance images of the brain using iterative clustering. *Magn. Reson. Imag.*, **23**(8):877-885. [doi:10.1016/j.mri.2005.07.010]

Hasanzadeh, M., Kasaei, S., 2007. Multispectral Brain MRI Segmentation Based on Fuzzy Classifiers and Evidence Theory. 15th Iranian Conf. on Electrical Engineering, p.1-5.

Heinonen, T., Dastidar, P., Eskola, H., Frey, H., Ryymin, P., Laasonen, E., 1998. Applicability of semi-automatic segmentation for volumetric analysis of brain lesions. *J. Med. Eng. Technol.*, **22**(4):173-178. [doi:10.3109/03091909809032536]

Ji, L., Yan, H., 2002. An attractable snakes based on the greedy algorithm for contour extraction. *Pattern Recogn.*, **35**(4):791-806. [doi:10.1016/S0031-3203(01)00085-1]

Ji, Z.X., Sun, Q.S., Xia, D.S., 2011. A modified possibilistic fuzzy c-means clustering algorithm for bias field estimation and segmentation of brain MR image. *Comput. Med. Imag. Graph.*, **35**(5):383-397. [doi:10.1016/j.compmedimag.2010.12.001]

Liew, A.W., Yan, H., 2003. An adaptive spatial fuzzy clustering algorithm for 3-D MR image segmentation. *IEEE Trans. Med. Imag.*, **22**(9):1063-1075. [doi:10.1109/TMI.2003.816956]

Liew, A.W., Yan, H., 2006. Current methods in the automatic tissue segmentation of 3D magnetic resonance brain images. *Curr. Med. Imag. Rev.*, **2**(1):91-103. [doi:10.2174/157340506775541604]

Lin, T.C., 2010. Switching-based filter based on Dempster's combination rule for image processing. *Inf. Sci.*, **180**(24):4892-4908. [doi:10.1016/j.ins.2010.08.011]

McInerney, T., Terzopoulos, D., 1996. Deformable models in medical image analysis: a survey. *Med. Image Anal.*, **1**(2):91-108. [doi:10.1016/S1361-8415(96)80007-7]

Niessen, W.J., Vincken, K.L., Weickert, J., Romeny, M.T.H., Viergever, M.A., 1999. Multiscale segmentation of three-dimensional MR brain images. *Int. J. Comput. Vis.*, **31**(2/3):185-202. [doi:10.1023/A:1008070000018]

Pham, D.L., Prince, J.L., 1999a. An adaptive fuzzy c-means algorithm for image segmentation in the presence of intensity inhomogeneities. *Pattern Recogn. Lett.*, **20**(1):57-68. [doi:10.1016/S0167-8655(98)00121-4]

Pham, D.L., Prince, J.L., 1999b. Adaptive fuzzy segmentation of magnetic resonance images. *IEEE Trans. Med. Imag.*, **18**(9):737-752. [doi:10.1109/42.802752]

Pham, D.L., Xu, C., Prince, J.L., 2000. A survey of current methods in medical image segmentation. *Ann. Rev. Biomed. Eng.*, **2**(1):315-337. [doi:10.1146/annurev.bioeng.2.1.315]

Prima, S., Ayache, N., Barrick, T., Roberts, N., 2001. Maximum Likelihood Estimation of the Bias Field in MR Brain Images: Investigating Different Modelings of the Imaging Process. Proc. 4th Int. Conf. on Medical Image Computing and Computer-Assisted Intervention, p.811-819.

Rakar, A., Juricic, D., Ballé, P., 1999. Transferable belief model in fault diagnosis. *Eng. Appl. Artif. Intell.*, **12**(5):555-567. [doi:10.1016/S0952-1976(99)00030-5]

Scherrer, B., Forbes, F., Garbay, C., Dojat, M., 2010. A joint Bayesian framework for MR brain scan tissue and structure segmentation based on distributed Markovian agents. *Comput. Intell. Healthcare 4*, **309**:81-101. [doi:10.1007/978-3-642-14464-6_5]

Shafer, G., 1976. A Mathematical Theory of Evidence. Princeton University Press, Princeton.

Shen, S., Sandham, W., Granat, M., Sterr, A., 2005. MRI fuzzy segmentation of brain tissue using neighborhood attraction with neural-network optimization. *IEEE Trans. Inf. Technol. Biomed.*, **9**(3):459-467. [doi:10.1109/TITB.2005.847500]

Simmons, A., Tofts, P.S., Barker, G.J., Arridge, S.R., 1994. Sources of intensity nonuniformity in spin echo images at 1.5 T. *Magn. Reson. Med.*, **32**(1):121-128. [doi:10.1002/mrm.1910320117]

Siyal, M.Y., Yu, L., 2005. An intelligent modified fuzzy c-means based algorithm for bias estimation and segmentation of brain MRI. *Pattern Recogn. Lett.*, **26**(13):2052-2062. [doi:10.1016/j.patrec.2005.03.019]

Sled, J.G., Zijdenbos, A.P., Evans, A.C., 1998. A non-parametric method for automatic correction of intensity nonuniformity in MRI data. *IEEE Trans. Med. Imag.*, **17**(1):87-97. [doi:10.1109/42.668698]

Styner, M., Brechbuhler, C., Szekely, G., Gerig, G., 2000. Parametric estimate of intensity inhomogeneities applied to MRI. *IEEE Trans. Med. Imag.*, **19**(3):153-165. [doi:10.1109/42.845174]

Tabassian, M., Ghaderi, R., Ebrahimpour, R., 2011. Knitted fabric defect classification for uncertain labels based on Dempster-Shafer theory of evidence. *Expert Syst. Appl.*, **38**(5):5259-5267. [doi:10.1016/j.eswa.2010.10.032]

Tabassian, M., Ghaderi, R., Ebrahimpour, R., 2012. Combination of multiple diverse classifiers using belief functions for handling data with imperfect labels. *Expert Syst. Appl.*, **39**(2):1698-1707. [doi:10.1016/j.eswa.2011.06.061]

Tsang, O., Gholipour, A., Kehtarnavaz, N., Panahi, I., Gopinath, K., Briggs, R., 2008. Comparison of Tissue Segmentation Algorithms in Neuroimage Analysis Software Tools. Proc. 30th Annual Int. Conf. of the IEEE Engineering in Medicine and Biology Society, p.3924-3928. [doi:10.1109/IEMBS.2008.4650068]

Valente, F., 2010. Multi-stream speech recognition based on Dempster-Shafer combination rule. *Speech Commun.*, **52**(3):213-222. [doi:10.1016/j.specom.2009.10.002]

Wang, J., Kong, J., Lu, Y., Qi, M., Zhang, B., 2008. A modified FCM algorithm for MRI brain image segmentation using both local and non-local spatial constraints. *Comput. Med. Imag. Graph.*, **32**(8):685-698. [doi:10.1016/j.compmedimag.2008.08.004]

Yager, R.R., Kacprzyk, J., Fedrizzi, M., 1994. Advances in the Dempster-Shafer Theory of Evidence. Wiley, Chichester.

Yoon, O.K., Kwak, D.M., Kim, D.W., Park, K.H., 1999. MR Brain Image Segmentation Using Fuzzy Clustering. Proc. IEEE Int. Fuzzy Systems Conf., **2**:853-857. [doi:10.1109/FUZZY.1999.793060]

Zhang, D.Q., Chen, S.C., 2004. A novel kernelized fuzzy c-means algorithm with application in medical image segmentation. *Artif. Intell. Med.*, **32**(1):37-50. [doi:10.1016/j.artmed.2004.01.012]